Mechanics of ultra-stretchable self-similar serpentine interconnects

Yihui Zhang [a,b,c,d,e,1], Haoran Fu [f,a,b,c,d,1], Yewang Su [a,b,c,d,e], Sheng Xu [g,h],
Huanyu Cheng [a,b,c,d], Jonathan A. Fan [g,h], Keh-Chih Hwang [e], John A. Rogers [g,h,*],
Yonggang Huang [a,b,c,d,*]

[a] *Department of Civil and Environmental Engineering, Northwestern University, Evanston, IL 60208, USA*
[b] *Department of Mechanical Engineering, Northwestern University, Evanston, IL 60208, USA*
[c] *Center for Engineering and Health, Northwestern University, Evanston, IL 60208, USA*
[d] *Skin Disease Research Center, Northwestern University, Evanston, IL 60208, USA*
[e] *Center for Mechanics and Materials, Tsinghua University, Beijing 100084, China*
[f] *Department of Civil Engineering and Architecture, Zhejiang University, Hangzhou 310058, China*
[g] *Department of Materials Science and Engineering, University of Illinois at Urbana–Champaign, Urbana, IL 61801, USA*
[h] *Frederick Seitz Materials Research Laboratory, University of Illinois at Urbana–Champaign, Urbana, IL 61801, USA*

Abstract

Electrical interconnects that adopt self-similar, serpentine layouts offer exceptional levels of stretchability in systems that consist of collections of small, non-stretchable active devices in the so-called island–bridge design. This paper develops analytical models of flexibility and elastic stretchability for such structures, and establishes recursive formulae at different orders of self-similarity. The analytic solutions agree well with finite element analysis, with both demonstrating that the elastic stretchability more than doubles when the order of the self-similar structure increases by one. Design optimization yields 90% and 50% elastic stretchability for systems with surface filling ratios of 50% and 70% of active devices, respectively.
© 2013 Acta Materialia Inc. Published by Elsevier Ltd. All rights reserved.

Keywords: Stretchable electronics; Serpentine interconnect; Mechanical properties; Self-similarity; Analytical modeling

1. Introduction

Interest in the development of electronic and optoelectronic systems that offer elastic response to large strain ($\gg 1\%$) deformation has grown rapidly in recent years [1–10], due in part to a range of important application possibilities that cannot be addressed with established technologies, such as wearable photovoltaics [11], "epidermal" health/wellness monitors [8], eyeball-like digital cameras [9,12] and sensitive robotic skins [13–15]. Many of these stretchable devices adopt the island–bridge design [8,12,16–18], where the active components are distributed in small, localized regions (i.e. islands) and are joined by narrow, deformable electrical and/or mechanical interconnects (i.e. bridges). Under stretching conditions, the relatively stiff islands effectively isolate the active components (usually brittle materials) from strains that could cause fracture (e.g. <1%); the bridge structures accommodate nearly all of the deformation [17–19]. For many practical devices, the island–bridge design must achieve simultaneously two competing goals, i.e. high surface filling ratio of active devices, and high stretchability of the entire

---

* Corresponding authors. Address: Department of Materials Science and Engineering, University of Illinois at Urbana–Champaign, Urbana, IL 61801, USA (J.A. Rogers). Department of Civil and Environmental Engineering, Northwestern University, Evanston, IL 60208, USA (Y. Huang).

E-mail addresses: jrogers@illinois.edu (J.A. Rogers), y-huang@northwestern.edu (Y. Huang).

[1] These authors contributed equally to this work.

system. Demonstrated design solutions involve either serpentine [1,8,17,20–27] or non-coplanar [12,18] interconnects. These technologies, however, typically give levels of total stretchability that are less than 50%, in systems that do not significantly sacrifice areal coverage. Recently, Xu et al. [19] illustrated an alternative type of interconnect design that exploits self-similar serpentine geometries (shown in Fig. 1a), a type of space-filling curve. This concept enabled lithium-ion batteries with a biaxial stretchability of up to ~300%, and areal coverages of active materials as high as ~50%. Comprehensive experimental and numerical investigations indicated that such self-similar serpentine interconnects possess improved levels of stretchability compared to traditional serpentine structures for a given spacing between adjacent islands. The nature of the

space-filling geometry in these structures and the mechanisms for their ordered unraveling were found to play important roles.

This study aims at developing an analytic model to study the flexibility and elastic stretchability (referred to simply as stretchability in the following) of self-similar serpentine interconnects, and to establish the design guidelines for optimizing the stretching limit. Here, we focus on the scenario that the interconnects are not bonded to the supporting substrate such that deformation can occur freely and the interactions with the substrate can be neglected. Such freely suspended interconnects can be fabricated by either of two methods: (i) molding surface relief structures on the elastomeric substrate [16,18,28] and bonding the islands onto the top of the raised relief; or (ii) designing
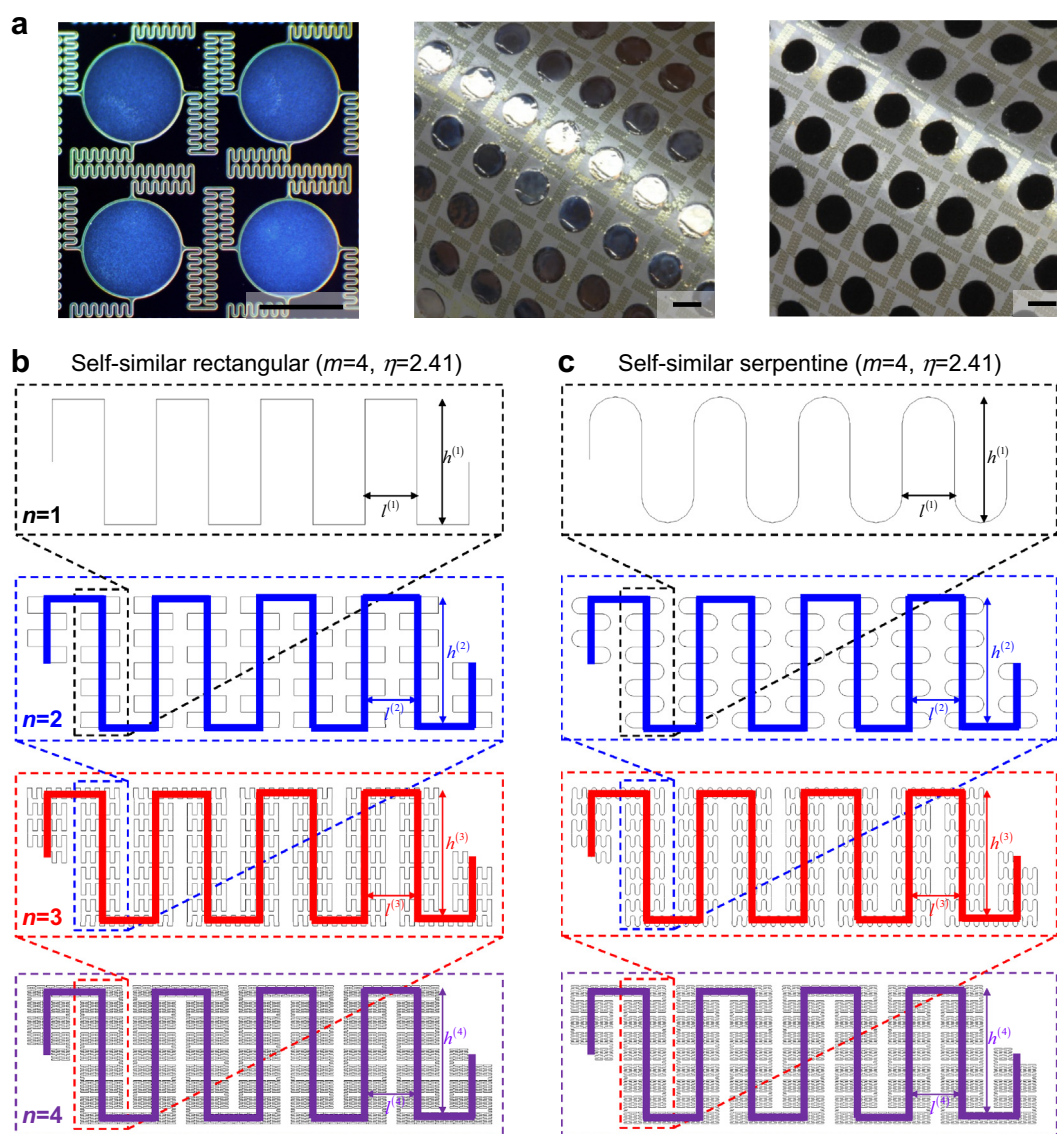

Fig. 1. (a) Optical images of the Al electrode pads and self-similar interconnects on Si wafer (left panel; top down view; ~4 unit cells), after transfer printing on a sheet of silicone (middle panel; oblique view, in a bent geometry), and with molded slurries of $LiCoO_2$ (right panel; oblique view, in a bent geometry), for a stretchable Li-ion battery; (b) schematic illustration on the geometric construction of the self-similar rectangular interconnect; (c) schematic illustration on the geometric construction of the self-similar serpentine interconnect. The scale bars in (a) are 2 mm. (a) is reprinted with permission from Xu et al. [19], © 2013, Nature Publishing Group.

the mask of SiO_2 deposition to enable selective bonding of the islands onto the substrate [29,30], while leaving the interconnects with a minimum interaction with the substrate. The present study mainly focuses on relative thick interconnects with the thickness comparable to the width, as required for applications that demand low electrical resistance, such as wireless inductive coils [19], and photovoltaic modules [11]. In such cases, the deformation of the interconnects is governed by in-plane bending, rather than buckling, when the system is under stretching. Here, the critical buckling strain is large compared to the stretchability [31], such that buckling is not triggered within the range of acceptable deformations. This mechanics is qualitatively different from that of the types of free-standing, thin serpentine interconnects that have been investigated previously [17,31–33]. For free-standing, thick self-similar interconnects, analytic models of the flexibility and stretchability are established in this study. The models are then extended to arbitrary self-similar orders. The results establish design guidelines for practical applications.

This paper is outlined as follows: Section 2 focuses on the simplest geometric configuration, self-similar rectangular interconnects, to illustrate the mechanics model for analyzing the flexibility and stretchability. The analytic model is extended to generalized self-similar rectangular and serpentine interconnects in Section 3. The stretchability of self-similar interconnects is studied in Section 4. Section 5 presents the optimal design of self-similar serpentine interconnects for stretchable electronics to illustrate its advantage in achieving high system stretchability.

2. Self-similar rectangular interconnects

This section focuses on a geometrically simple self-similar interconnect in a rectangular configuration (as shown in Fig. 1b), to illustrate its structure, flexibility and stretchability. The rectangular interconnect is a variant of the traditional serpentine interconnect (top panel of Fig. 1c), and is convenient for constructing self-similar structures because of its simple geometry. To determine the flexibility of self-similar rectangular interconnects, the key is to establish the relation between the flexibility of neighboring orders, i.e. the recursion formula. We first take the first order self-similar rectangular interconnect as an example to illustrate the model as in Section 2.2, and then generalize the theoretical framework to the second order and arbitrary order in Sections 2.3 and 2.4, respectively.

2.1. Geometry

This subsection introduces the geometric construction of self-similar rectangular interconnects. The first order (original) rectangular interconnect consists of two sets of straight wires that are perpendicular to each other and connected in series, as shown in the black box of Fig. 1b. The second order rectangular interconnect, shown in the blue box of

Fig. 1b, is created by reducing the scale of the first order interconnect, rotating the structure by 90° and then connecting multiple copies of it in a fashion that reproduces the layout of original geometry. The wide blue line in Fig. 1b represents the second order geometry that is similar to the first order rectangular geometry. By implementing the same algorithm, we can generate the third- and fourth order rectangular interconnects, as illustrated in the red and purple boxes of Fig. 1b, where the red and purple lines denote the third- and fourth order geometries, respectively.

For self-similar rectangular interconnects, let m denote the number of unit cell and η the height/spacing aspect ratio at each order. Therefore the lengths of horizontal and vertical lines of the ith order ($i = 1, \ldots, n$), $l^{(i)}$ and $h^{(i)}$ (Fig. 1b), are related by

$$h^{(i)} = \eta l^{(i)} \tag{1}$$

In addition, the height of ith order geometry equals to the distance between two ends of $(i − 1)$th order geometry, that is

$$h^{(i)} = 2m l^{(i-1)} \quad (i = 2, \ldots, n) \tag{2}$$

Eqs. (1) and (2) give the length and height at any order in terms of $l^{(n)}$, η and m, as

$$l^{(i)} = (\eta/2m)^{n-i} l^{(n)}, \quad h^{(i)} = \eta(\eta/2m)^{n-i} l^{(n)}, \quad (i = 1, \ldots, n) \tag{3}$$

This indicates that the geometry of an arbitrary self-similar rectangular interconnect is characterized by one base length ($l^{(n)}$) and three non-dimensional parameters, namely the self-similar order (n), the height/spacing ratio (η) and number (m) of unit cell. It should be mentioned that, for $n \geqslant 3$, there is an additional constraint on the height/spacing ratio η because of the following relation, which can be observed from the geometry of the third order rectangular interconnect shown in Figs. 1 and 3 (to be discussed):

$$l^{(i)} = (2m_h + 1)l^{(i-2)} \quad (i = 3, \ldots, n) \tag{4}$$

where m_h is the number of full unit cells in the structure represented by the horizontal part of the ith order geometry ($i = 3, \ldots, n$). Eqs. (3) and (4) give the constraint on the height/spacing ratio η for $n \geqslant 3$:

$$\eta = \frac{2m}{\sqrt{2m_h + 1}} \quad (i = 3, \ldots, n) \tag{5}$$

i.e. the height/spacing ratio can only take some discrete values for $n \geqslant 3$. Fig. 1b shows a set of self-similar rectangular interconnects, from $n=1$ to 4, with $m = 4$ and $\eta = 8/\sqrt{11}$.

2.2. Flexibility of first order rectangular interconnects

Fig. 2a shows a schematic illustration of the first order self-similar rectangular interconnect with m unit cells and height/spacing ratio η. As illustrated in Fig. 2b, a represen-
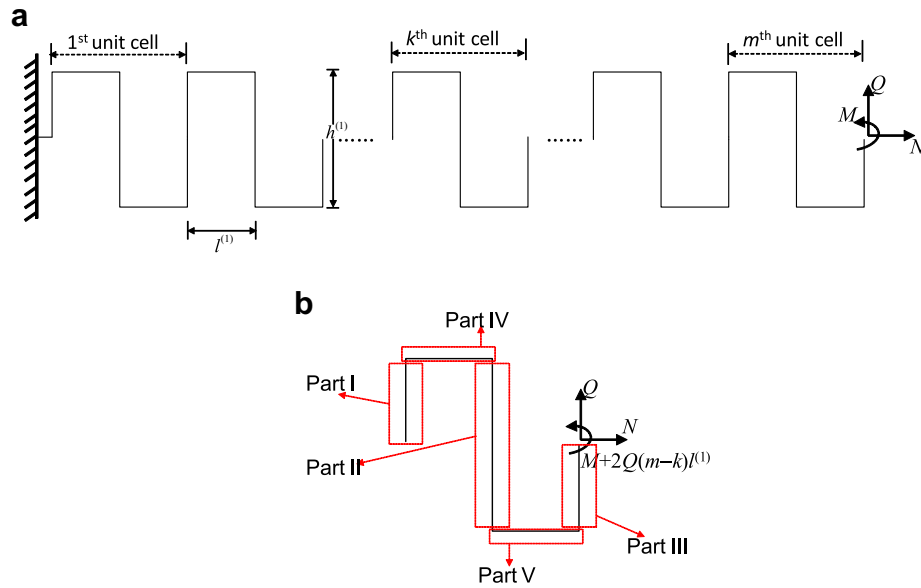
Fig. 2. (a) A freely suspended first order rectangular interconnect, clamped at the left end, and subject to an axial force N, shear force Q, and bending moment M, at the right end. (b) Exploded view and free body diagram of the kth unit cell of first order rectangular interconnect.
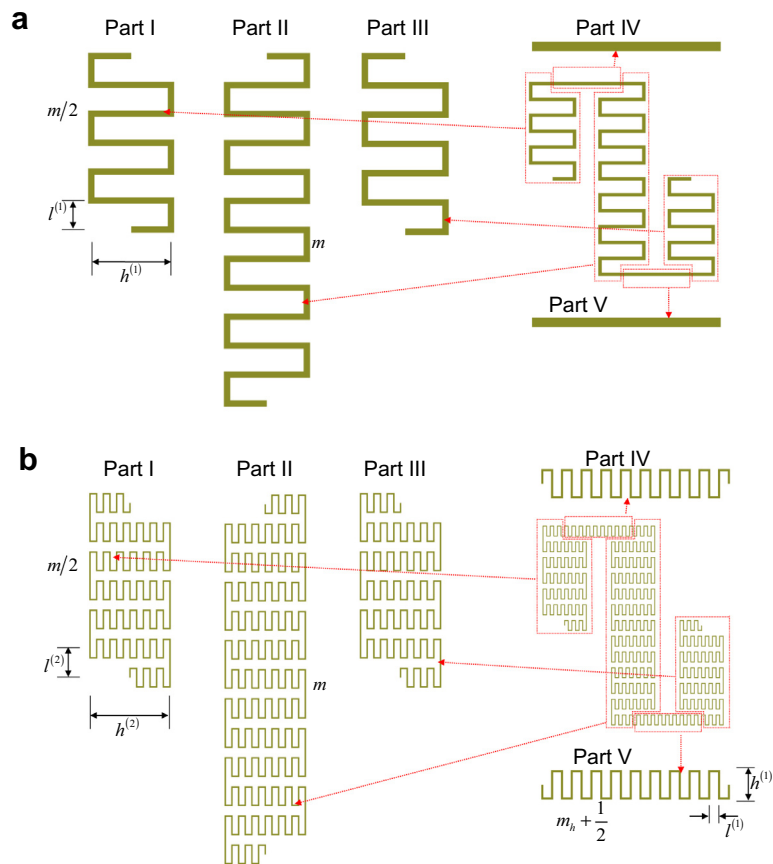

Fig. 3. The exploded view of a representative unit cell for the (a) second order and (b) third order self-similar rectangular interconnect.

tative unit cell (e.g. the kth unit cell) of the first order structure is composed of five straight wires (i.e. zeroth order structure) (Parts I–V). The vertical wires, Parts I and III, have a length of $h^{(1)}/2$, and Part II has a length of $h^{(1)}$. The horizontal wires, Parts IV and V, have a length of $l^{(1)}$.

Consider the first order rectangular interconnect clamped at the left end, and subject to an axial force N (along the direction between the two ends of the interconnect), a shear force Q (normal to N) and a bending moment M, at the right end, within the plane of interconnect, as shown in Fig. 2a. The width (w) and thickness (t) of the serpentine interconnect are usually much smaller than the length such that the structure can be modeled as a curved beam. Let u and v denote the displacements at the right end, along and normal to the axial direction of the interconnect (parallel to N and to Q), respectively, and θ is the rotation angle (Fig. 2a). They are related to (N, Q, M) via the strain energy $W^{(1)}$ in the interconnect by

$$\begin{pmatrix} u \\ v \\ \theta \end{pmatrix} = \begin{bmatrix} \partial W^{(1)}/\partial N \\ \partial W^{(1)}/\partial Q \\ \partial W^{(1)}/\partial M \end{bmatrix} = \begin{bmatrix} T_{11}^{(1)} & T_{12}^{(1)} & T_{13}^{(1)} \\ T_{12}^{(1)} & T_{22}^{(1)} & T_{23}^{(1)} \\ T_{13}^{(1)} & T_{23}^{(1)} & T_{33}^{(1)} \end{bmatrix} \begin{pmatrix} N \\ Q \\ M \end{pmatrix}$$

$$= \boldsymbol{T}^{(1)} \begin{pmatrix} N \\ Q \\ M \end{pmatrix} \tag{6}$$

where $W^{(1)} = (N, Q, M)\boldsymbol{T}^{(1)}(N, Q, M)^T/2$ is a quadratic function of N, Q, and M for linear elastic behavior of the interconnect; and $\boldsymbol{T}^{(1)}$ is the symmetric flexibility matrix of the first order interconnect and is to be determined. The strain energy also equals the sum of strain energy $W^{(0)}$ in all zeroth order interconnects (Parts I–V), i.e.

$$W^{(1)} = W^{(0)} = \sum_{k=1}^{m} \left(W_k^I + W_k^{II} + W_k^{III} + W_k^{IV} + W_k^V \right) \tag{7}$$

where W_k^I to W_k^V represent the strain energy of each component in the kth unit cell. For the zeroth order structure, i.e. a straight wire with length l and bending stiffness EI, the beam theory gives the flexibility matrix as [34]

$$\boldsymbol{T}^{(0)}(l) = \frac{1}{6EI} \begin{pmatrix} 0 & 0 & 0 \\ 0 & 2l^3 & 3l^2 \\ 0 & 3l^2 & 6l \end{pmatrix} \tag{8}$$

Here the membrane energy is neglected. The free body diagram of the kth unit cell of the first order interconnect (Fig. 2b) gives the axial force, shear force and bending moment in each wire, and the strain energy of each zeroth order interconnect can then be obtained as

$$\begin{pmatrix} W_k^I \\ W_k^{II} \\ W_k^{III} \\ W_k^{IV} \\ W_k^V \end{pmatrix} = \frac{1}{2}(N,Q,M) \begin{cases} \boldsymbol{D}_I \boldsymbol{T}^{(0)}[h^{(1)}/2]\boldsymbol{D}_I^T \\ \boldsymbol{D}_{II} \boldsymbol{T}^{(0)}[h^{(1)}]\boldsymbol{D}_{II}^T \\ \boldsymbol{D}_{III} \boldsymbol{T}^{(0)}[h^{(1)}/2]\boldsymbol{D}_{III}^T \\ \boldsymbol{D}_{IV} \boldsymbol{T}^{(0)}[l^{(1)}]\boldsymbol{D}_{IV}^T \\ \boldsymbol{D}_V \boldsymbol{T}^{(0)}[l^{(1)}]\boldsymbol{D}_V^T \end{cases} (N,Q,M)^T \tag{9}$$

where $\quad \boldsymbol{D}_I = \begin{bmatrix} 0 & 1 & -h^{(1)}/2 \\ 1 & 0 & -(2m-2k+2)l^{(1)} \\ 0 & 0 & -1 \end{bmatrix}$,

$$\boldsymbol{D}_{II} = \begin{bmatrix} 0 & 1 & -h^{(1)}/2 \\ -1 & 0 & (2m-2k+1)l^{(1)} \\ 0 & 0 & 1 \end{bmatrix},$$

$$\boldsymbol{D}_{III} = \begin{bmatrix} 0 & 1 & 0 \\ 1 & 0 & -(2m-2k)l^{(1)} \\ 0 & 0 & -1 \end{bmatrix},$$

$$\boldsymbol{D}_{IV} = \begin{bmatrix} 1 & 0 & h^{(1)}/2 \\ 0 & 1 & (2m-2k+1)l^{(1)} \\ 0 & 0 & 1 \end{bmatrix} \quad \text{and}$$

$$\boldsymbol{D}_V = \begin{bmatrix} 1 & 0 & h^{(1)}/2 \\ 0 & -1 & -(2m-2k)l^{(1)} \\ 0 & 0 & -1 \end{bmatrix} \tag{10}$$

Substitution of Eq. (9) into Eq. (7) gives the recursive formula between the flexibility matrices of first and zeroth order interconnects as

$$\boldsymbol{T}^{(1)} = \sum_{k=1}^{m} \left\{ \begin{array}{l} \boldsymbol{D}_I \boldsymbol{T}^{(0)}[h^{(1)}/2]\boldsymbol{D}_I^T + \boldsymbol{D}_{II} \boldsymbol{T}^{(0)}[h^{(1)}]\boldsymbol{D}_{II}^T \\ + \boldsymbol{D}_{III} \boldsymbol{T}^{(0)}[h^{(1)}/2]\boldsymbol{D}_{III}^T + \boldsymbol{D}_{IV} \boldsymbol{T}^{(0)}[l^{(1)}]\boldsymbol{D}_{IV}^T + \boldsymbol{D}_V \boldsymbol{T}^{(0)}[l^{(1)}]\boldsymbol{D}_V^T \end{array} \right\} \tag{11}$$

Substitution of $\boldsymbol{T}^{(0)}$ in Eq. (8) into the above equation gives a simple expression of the flexibility of first order interconnect in terms of the number of unit cells m, height/spacing ratio η and $l^{(1)}$:

$$\boldsymbol{T}^{(1)}\left[m,\eta,l^{(1)}\right]$$
$$= \frac{1}{EI} \left\{ \begin{array}{ccc} m\frac{\eta^3+3\eta^2}{6}[l^{(1)}]^3 & m\frac{\eta(\eta+2)}{4}[l^{(1)}]^3 & 0 \\ m\frac{\eta(\eta+2)}{4}[l^{(1)}]^3 & \frac{(8m^3+m)\eta+8m^3}{3}[l^{(1)}]^3 & 2m^2(\eta+1)[l^{(1)}]^2 \\ 0 & 2m^2(\eta+1)[l^{(1)}]^2 & 2m(\eta+1)l^{(1)} \end{array} \right\} \tag{12}$$

For the convenience of generalization to higher order (n) structure, the following non-dimensional form of flexibility matrix is adopted:

$$\begin{bmatrix} u/l^{(i)} \\ v/l^{(i)} \\ \theta \end{bmatrix} = \frac{l^{(i)}}{EI} \overline{\boldsymbol{T}}^{(i)} \begin{bmatrix} Nl^{(i)} \\ Ql^{(i)} \\ M \end{bmatrix}, \quad i = 1, \ldots, n \tag{13}$$

where $\overline{\boldsymbol{T}}^{(i)}$ is dimensionless, and $\overline{\boldsymbol{T}}^{(1)}$ is given by

$$\overline{\boldsymbol{T}}^{(1)}(m,\eta) = \begin{bmatrix} m\frac{\eta^3+3\eta^2}{6} & m\frac{\eta(\eta+2)}{4} & 0 \\ m\frac{\eta(\eta+2)}{4} & \frac{(8m^3+m)\eta+8m^3}{3} & 2m^2(\eta+1) \\ 0 & 2m^2(\eta+1) & 2m(\eta+1) \end{bmatrix} \tag{14}$$

For the zeroth order structure, i.e. a straight wire of length λ, the non-dimensional flexibility matrix is defined as $(u/\lambda, v/\lambda, \theta)^T = (\lambda/EI)\overline{\boldsymbol{T}}^{(0)}(N\lambda, Q\lambda, M)^T$, where

$$\overline{\boldsymbol{T}}^{(0)} = \begin{pmatrix} 0 & 0 & 0 \\ 0 & \frac{1}{3} & \frac{1}{2} \\ 0 & \frac{1}{2} & 1 \end{pmatrix} \tag{15}$$

2.3. Flexibility of the second order rectangular interconnect

The recursive formula for the flexibility matrix of the second order interconnect is established in this section. A representative unit cell of the second order structure is composed of three first order structures (Parts I–III), and two straight wires (i.e. zeroth order structure) (Parts IV and V) with length of $l^{(2)}$, as illustrated in Fig. 3a. The first order structures, Parts I and III, consist of $m/2$ (m is an even integer) unit cells, and Part II consists of m unit cells.

The strain energy of the second order structure can be expressed in terms of the dimensionless flexibility matrix as

$$W^{(2)} = \frac{l^{(2)}}{2EI} [Nl^{(2)}, Ql^{(2)}, M] \overline{\boldsymbol{T}}^{(2)} [Nl^{(2)}, Ql^{(2)}, M]^T$$
$$= \frac{l^{(2)}}{2EI} (N, Q, M) \begin{bmatrix} l^{(2)} & 0 & 0 \\ 0 & l^{(2)} & 0 \\ 0 & 0 & 1 \end{bmatrix} \overline{\boldsymbol{T}}^{(2)} \begin{bmatrix} l^{(2)} & 0 & 0 \\ 0 & l^{(2)} & 0 \\ 0 & 0 & 1 \end{bmatrix} (N, Q, M)^T \tag{16}$$

where $\overline{\boldsymbol{T}}^{(2)}$ is to be determined. The strain energy also equals the sum of strain energy in all first order (Parts I–III, Fig. 3a) and zeroth order (Parts IV and V, Fig. 3a) interconnects, i.e.

$$W^{(2)} = \sum_{k=1}^{m} (W_k^I + W_k^{II} + W_k^{III} + W_k^{IV} + W_k^V) \tag{17}$$

where

$$W_k^{II} = \frac{l^{(1)}}{2EI} [Nl^{(1)}, Ql^{(1)}, M] \overline{\boldsymbol{D}}_{II} \overline{\boldsymbol{T}}^{(1)}(m, \eta) \overline{\boldsymbol{D}}_{II}^T [Nl^{(1)}, Ql^{(1)}, M]^T \tag{18}$$

is the strain energy in Part II (first order structure, m unit cell) with $\overline{\boldsymbol{D}}_{II} = \begin{bmatrix} 0 & 1 & -m \\ -1 & 0 & (4m - 4k + 2)mn^{-1} \\ 0 & 0 & 1 \end{bmatrix}$ being the normalized $\boldsymbol{D}_{II}$ in Eq. (10) (with $l^{(1)}$ and $h^{(1)}$ replaced by $l^{(2)}$ and $h^{(2)}$, respectively);

$$W_k^{IV} = \frac{l^{(2)}}{2EI} [Nl^{(2)}, Ql^{(2)}, M] \overline{\boldsymbol{D}}_{IV} \overline{\boldsymbol{T}}^{(0)} \overline{\boldsymbol{D}}_{IV}^T [Nl^{(2)}, Ql^{(2)}, M]^T$$
$$W_k^V = \frac{l^{(2)}}{2EI} [Nl^{(2)}, Ql^{(2)}, M] \overline{\boldsymbol{D}}_V \overline{\boldsymbol{T}}^{(0)} \overline{\boldsymbol{D}}_V^T [Nl^{(2)}, Ql^{(2)}, M]^T \tag{19}$$

are the strain energy in Parts IV and V (zeroth order structure, length $\lambda = l^{(2)}$) with $\overline{\boldsymbol{D}}_{IV} = \begin{pmatrix} 1 & 0 & \eta/2 \\ 0 & 1 & 2m - 2k + 1 \\ 0 & 0 & 1 \end{pmatrix}$

and $\overline{\boldsymbol{D}}_V = \begin{pmatrix} 1 & 0 & \eta/2 \\ 0 & -1 & -2m + 2k \\ 0 & 0 & -1 \end{pmatrix}$ being the normalized $\boldsymbol{D}_{IV}$ and $\boldsymbol{D}_V$ in Eq. (10) (with $l^{(1)}$ and $h^{(1)}$ replaced by $l^{(2)}$ and $h^{(2)}$, respectively);

$$W_k^I = \frac{l^{(1)}}{2EI} [Nl^{(1)}, Ql^{(1)}, M] \overline{\boldsymbol{D}}_I \overline{\boldsymbol{T}}^{(1)} \left(\frac{m}{2}, \eta\right) \overline{\boldsymbol{D}}_I^T [Nl^{(1)}, Ql^{(1)}, M]^T$$
$$W_k^{III} = \frac{l^{(1)}}{2EI} [Nl^{(1)}, Ql^{(1)}, M] \overline{\boldsymbol{D}}_{III} \overline{\boldsymbol{T}}^{(1)} \left(\frac{m}{2}, \eta\right) \overline{\boldsymbol{D}}_{III}^T [Nl^{(1)}, Ql^{(1)}, M]^T \tag{20}$$

are the strain energy in Parts I and III (first order structure, $m/2$ unit cell) with $\overline{\boldsymbol{D}}_I = \begin{bmatrix} 0 & 1 & -m \\ 1 & 0 & -4(m - k + 1)mn^{-1} \\ 0 & 0 & -1 \end{bmatrix}$ and

$\overline{\boldsymbol{D}}_{III} = \begin{bmatrix} 0 & 1 & 0 \\ 1 & 0 & -4(m - k)mn^{-1} \\ 0 & 0 & -1 \end{bmatrix}$ being the normalized $\boldsymbol{D}_I$ and $\boldsymbol{D}_{III}$ in Eq. (10) [with $l^{(1)}$ and $h^{(1)}$ replaced by $l^{(2)}$ and $h^{(2)}$, respectively].

Substitution of Eqs. (18)–(20) into Eq. (17) gives the recursive formula for the flexibility matrix of second order interconnect as

$$\overline{\boldsymbol{T}}^{(2)} = \frac{\eta}{2m} \begin{pmatrix} \frac{\eta}{2m} & 0 & 0 \\ 0 & \frac{\eta}{2m} & 0 \\ 0 & 0 & 1 \end{pmatrix}$$
$$\times \sum_{k=1}^{m} \left\{ \begin{array}{c} \overline{\boldsymbol{D}}_I [\overline{\boldsymbol{T}}^{(1)} \boldsymbol{K}(m\eta) + \boldsymbol{K}^T(m\eta) \overline{\boldsymbol{T}}^{(1)}] \overline{\boldsymbol{D}}_I^T + \overline{\boldsymbol{D}}_{II} \overline{\boldsymbol{T}}^{(1)} \overline{\boldsymbol{D}}_{II}^T \\ + \overline{\boldsymbol{D}}_{III} [\overline{\boldsymbol{T}}^{(1)} \boldsymbol{K}(m\eta) + \boldsymbol{K}^T(m\eta) \overline{\boldsymbol{T}}^{(1)}] \overline{\boldsymbol{D}}_{III}^T \end{array} \right\}$$
$$\times \begin{pmatrix} \frac{\eta}{2m} & 0 & 0 \\ 0 & \frac{\eta}{2m} & 0 \\ 0 & 0 & 1 \end{pmatrix} + \sum_{k=1}^{m} [\overline{\boldsymbol{D}}_{IV} \overline{\boldsymbol{T}}^{(0)} \overline{\boldsymbol{D}}_{IV}^T + \overline{\boldsymbol{D}}_V \overline{\boldsymbol{T}}^{(0)} \overline{\boldsymbol{D}}_V^T] \tag{21}$$

where

$$\boldsymbol{K}(m\eta) = \frac{1}{4} \begin{pmatrix} 1 & 0 & 0 \\ 0 & 1 & 0 \\ 0 & -m\eta & 1 \end{pmatrix} \tag{22}$$

results from the identity

$$\overline{\boldsymbol{T}}^{(1)} \left(\frac{m}{2}, \eta\right) = \overline{\boldsymbol{T}}^{(1)}(m, \eta) \boldsymbol{K}(m\eta) + \boldsymbol{K}^T(m\eta) \overline{\boldsymbol{T}}^{(1)}(m, \eta) \tag{23}$$

Substitution of $\overline{\boldsymbol{T}}^{(0)}$ and $\overline{\boldsymbol{T}}^{(1)}$ in Eqs. (15) and (14) into Eq. (21) gives $\overline{\boldsymbol{T}}^{(2)}$ as

$$\overline{\boldsymbol{T}}^{(2)}(m, \eta) = \begin{bmatrix} \eta^2 \frac{\eta^2 + 2m^2(f+2)}{12m} & \frac{m}{4} \eta(f + 1) & 0 \\ \frac{m}{4} \eta(f + 1) & \frac{\eta^5(\eta+3) + 8m^2(f-1) + 64m^4 f}{24m} & 2m^2 f \\ 0 & 2m^2 f & 2mf \end{bmatrix} \tag{24}$$
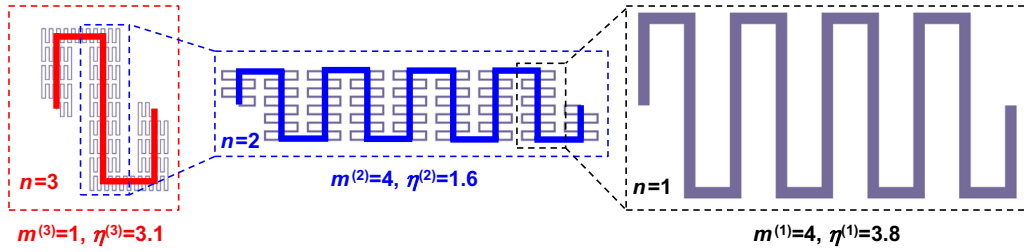
where $f = \eta^2 + \eta + 1$.

Fig. 4. Schematic illustration on the geometric construction of a third order generalized self-similar serpentine interconnect.

2.4. Flexibility of higher order rectangular interconnect

For the higher order ($n \geq 3$) rectangular interconnect, a representative unit cell is composed of three $(n-1)$ order structures (Parts I–III), and two $(n-2)$ order structures (Parts IV and V). The $(n-1)$ order structures, Parts I and III, consist of $m/2$ (m is an even integer) unit cells, and Part II consists of m unit cells. The recursive formula (21) becomes[2]

$$
\overline{T}^{(n)} = \frac{\eta}{2m} \begin{pmatrix} \frac{\eta}{2m} & 0 & 0 \\ 0 & \frac{\eta}{2m} & 0 \\ 0 & 0 & 1 \end{pmatrix}
$$
$$
\times \sum_{k=1}^{m} \left\{ \begin{array}{c} \overline{D}_I \left[\overline{T}^{(n-1)} K(m\eta) + K^T(m\eta) \overline{T}^{(n-1)} \right] \overline{D}_I^T \\ + \overline{D}_{II} \overline{T}^{(n-1)} \overline{D}_{II}^T \\ + \overline{D}_{III} \left[\overline{T}^{(n-1)} K(m\eta) + K^T(m\eta) \overline{T}^{(n-1)} \right] \overline{D}_{III}^T \end{array} \right\}
$$
$$
\times \begin{pmatrix} \frac{\eta}{2m} & 0 & 0 \\ 0 & \frac{\eta}{2m} & 0 \\ 0 & 0 & 1 \end{pmatrix} + \frac{\eta^2}{4m^2} \sum_{k=1}^{m} \left[\overline{D}_{IV}^* \overline{T}^{(n-2)} \overline{D}_{IV}^{*T} + \overline{D}_V^* \overline{T}^{(n-2)} \overline{D}_V^{*T} \right] \text{ for } n \geq 3 \quad (25)
$$

where $\overline{D}_{IV}^* = \begin{bmatrix} \eta^2/(4m^2) & 0 & \eta/2 \\ 0 & \eta^2/(4m^2) & 2m - 2k + 1 \\ 0 & 0 & 1 \end{bmatrix}$ and

$\overline{D}_V^* = \begin{bmatrix} \eta^2/(4m^2) & 0 & \eta/2 \\ 0 & -\eta^2/(4m^2) & -2m + 2k \\ 0 & 0 & -1 \end{bmatrix}$

3. Generalized self-similar interconnects

The analytic model for self-similar rectangular interconnects in Section 2 is extended to generalized self-similar rectangular and serpentine interconnects in this section.

3.1. Generalized self-similar rectangular interconnects

The generalized rectangular interconnect still exhibits the rectangular shape (shown in Fig. 4), but does not require the same height/spacing ratio across different orders, nor the number of unit cell. Each order may have

its own height/spacing ratio $\eta^{(i)}$ and number of unit cell $m^{(i)}$ ($i = 1, \ldots, n$), where only $m^{(n)}$ can be an odd number, and $m^{(1)}$ to $m^{(n)}$ must be even numbers. Fig. 4 illustrates a generalized third order self-similar rectangular interconnect. For the nth order generalized self-similar rectangular interconnect, the geometric relations (1)–(3) become

$$ h^{(i)} = \eta^{(i)} l^{(i)} \quad (26) $$

$$ h^{(i)} = 2m^{(i-1)} l^{(i-1)} \quad (i = 2, \ldots, n) \quad (27) $$

$$ l^{(i)} = \left[\prod_{k=1}^{n-i} \frac{\eta^{(n-k+1)}}{2m^{(n-k)}} \right] l^{(n)}, h^{(i)} $$
$$ = \eta^{(i)} \left[\prod_{k=1}^{n-i} \frac{\eta^{(n-k+1)}}{2m^{(n-k)}} \right] l^{(n)}, \quad (i = 1, \ldots, n-1) \quad (28) $$

The flexibility matrix $\overline{T}^{(0)}$ in Eq. (15) remains the same, while m and η in Eq. (14) for $\overline{T}^{(1)}$ need to be replaced by $m^{(1)}$ and $\eta^{(1)}$, respectively. The recursive formulae for $\overline{T}^{(2)}$ in Eq. (21) and $\overline{T}^{(n)}$ ($n \geq 3$) in Eq. (25) now become

$$
\overline{T}^{(2)} = \frac{\eta^{(2)}}{2m^{(1)}} \begin{bmatrix} \frac{\eta^{(2)}}{2m^{(1)}} & 0 & 0 \\ 0 & \frac{\eta^{(2)}}{2m^{(1)}} & 0 \\ 0 & 0 & 1 \end{bmatrix}
$$
$$
\times \sum_{k=1}^{m^{(2)}} \left\langle \begin{array}{c} \overline{D}_I^{(2)} \left\{ \begin{array}{c} \overline{T}^{(1)} K\left[m^{(1)} \eta^{(1)}\right] \\ + K^T\left[m^{(1)} \eta^{(1)}\right] \overline{T}^{(1)} \end{array} \right\} \overline{D}_I^{(2)T} \\ + \overline{D}_{II}^{(2)} \overline{T}^{(1)} \overline{D}_{II}^{(2)T} \\ + \overline{D}_{III}^{(2)} \left\{ \begin{array}{c} \overline{T}^{(1)} K\left[m^{(1)} \eta^{(1)}\right] \\ + K^T\left[m^{(1)} \eta^{(1)}\right] \overline{T}^{(1)} \end{array} \right\} \overline{D}_{III}^{(2)T} \end{array} \right\rangle \begin{bmatrix} \frac{\eta^{(2)}}{2m^{(1)}} & 0 & 0 \\ 0 & \frac{\eta^{(2)}}{2m^{(1)}} & 0 \\ 0 & 0 & 1 \end{bmatrix}
$$
$$
+ \sum_{k=1}^{m^{(2)}} \left[\overline{D}_{IV}^{(2)} \overline{T}^{(0)} \overline{D}_{IV}^{(2)T} + \overline{D}_V^{(2)} \overline{T}^{(0)} \overline{D}_V^{(2)T} \right] \quad (29)
$$

$$
\overline{T}^{(n)} = \frac{\eta^{(n)}}{2m^{(n-1)}} \begin{bmatrix} \frac{\eta^{(n)}}{2m^{(n-1)}} & 0 & 0 \\ 0 & \frac{\eta^{(n)}}{2m^{(n-1)}} & 0 \\ 0 & 0 & 1 \end{bmatrix}
$$
$$
\times \sum_{k=1}^{m^{(n)}} \left\langle \begin{array}{c} \overline{D}_I^{(n)} \left\{ \begin{array}{c} \overline{T}^{(n-1)} K\left[m^{(n-1)} \eta^{(n-1)}\right] \\ + K^T\left[m^{(n-1)} \eta^{(n-1)}\right] \overline{T}^{(n-1)} \end{array} \right\} \overline{D}_I^{(n)T} \\ + \overline{D}_{II}^{(n)} \overline{T}^{(n-1)} \overline{D}_{II}^{(n)T} \\ + \overline{D}_{III}^{(n)} \left\{ \begin{array}{c} \overline{T}^{(n-1)} K\left[m^{(n-1)} \eta^{(n-1)}\right] \\ + K^T\left[m^{(n-1)} \eta^{(n-1)}\right] \overline{T}^{(n-1)} \end{array} \right\} \overline{D}_{III}^{(n)T} \end{array} \right\rangle \cdot \begin{bmatrix} \frac{\eta^{(n)}}{2m^{(n-1)}} & 0 & 0 \\ 0 & \frac{\eta^{(n)}}{2m^{(n-1)}} & 0 \\ 0 & 0 & 1 \end{bmatrix}
$$
$$
+ \frac{\eta^{(n)} \eta^{(n-1)}}{4m^{(n-1)} m^{(n-2)}} \sum_{k=1}^{m^{(n)}} \left[\overline{D}_{IV}^{(n)*} \overline{T}^{(n-2)} \overline{D}_{IV}^{(n)*T} + \overline{D}_V^{(n)*} \overline{T}^{(n-2)} \overline{D}_V^{(n)*T} \right], \text{ for } n \geq 3 \quad (30)
$$

---

[2] The $(n-2)$th order structures (e.g. Parts IV and V in Fig. 3b for the case of $n = 3$) have $(m_h + 1/2)$ unit cells at the $(n-2)$th order geometry. However, because the contribution of the $(n-2)$th order structures to the overall flexibility is much smaller than that of $(n-1)$th order structures, the dimensionless flexibility of Parts IV and V can be approximated by the self-similar $(n-2)$th order structures with m unit cells, which, as to be shown by finite element analysis, gives rather good accuracy.

where

$$\overline{D}_I^{(n)} = \left\{ \begin{array}{ccc} 0 & 1 & -m^{(n-1)} \\ 1 & 0 & -4[m^{(n)}-k+1]m^{(n-1)}[\eta^{(n)}]^{-1} \\ 0 & 0 & -1 \end{array} \right\},$$

$$\overline{D}_{II}^{(n)} = \left\{ \begin{array}{ccc} 0 & 1 & -m^{(n-1)} \\ -1 & 0 & [4m^{(n)}-4k+2]m^{(n-1)}[\eta^{(n)}]^{-1} \\ 0 & 0 & 1 \end{array} \right\}$$

$$\text{and } \overline{D}_{III}^{(n)} = \left[\begin{array}{ccc} 0 & 1 & 0 \\ 1 & 0 & -4[m^{(n)}-k]m^{(n-1)}[\eta^{(n)}]^{-1} \\ 0 & 0 & -1 \end{array} \right] \quad \text{for } n \geqslant 2$$

$$\overline{D}_{IV}^{(2)} = \left[\begin{array}{ccc} 1 & 0 & \eta^{(2)}/2 \\ 0 & 1 & 2m^{(2)}-2k+1 \\ 0 & 0 & 1 \end{array} \right],$$

$$\overline{D}_V^{(2)} = \left[\begin{array}{ccc} 1 & 0 & \eta^{(2)}/2 \\ 0 & -1 & -2m^{(2)}+2k \\ 0 & 0 & -1 \end{array} \right] \quad \text{and}$$

$$\overline{D}_{IV}^{*(n)} = \left[\begin{array}{ccc} \eta^{(n-1)}\eta^{(n)}/[4m^{(n-2)}m^{(n-1)}] & 0 & \eta^{(n)}/2 \\ 0 & \eta^{(n-1)}\eta^{(n)}/[4m^{(n-2)}m^{(n-1)}] & 2m^{(n)}-2k+1 \\ 0 & 0 & 1 \end{array} \right]$$

$$\text{and } \overline{D}_V^{*(n)} = \left[\begin{array}{ccc} \eta^{(n-1)}\eta^{(n)}/[4m^{(n-2)}m^{(n-1)}] & 0 & \eta^{(n)}/2 \\ 0 & -\eta^{(n-1)}\eta^{(n)}/[4m^{(n-2)}m^{(n-1)}] & -2m^{(n)}+2k \\ 0 & 0 & -1 \end{array} \right]$$

$$\text{for } n \geqslant 3$$

3.2. Generalized self-similar serpentine interconnects

Fig. 1b and c shows the generalized self-similar serpentine interconnect, which replaces the sharp corners in the rectangular configuration by half circles, as in Xu et al.'s experiments [19]. The first order serpentine interconnect consists of straight wires (length $h^{(1)}-l^{(1)}$) connected by half circles (diameter $l^{(1)}$), as shown in the black box of Fig. 1c. A representative unit cell of the second order serpentine interconnect, as shown in the blue box of Fig. 1c, is composed of two (horizontal) straight wires of length $l^{(2)}$ and

three (vertical) first order serpentine interconnects (two with lengths $h^{(2)}/2$ and one with length of $h^{(2)}$). The flexibility matrix $\overline{T}^{(0)}$ for straight wires is still given in Eq. (15), and the flexibility matrix $\overline{T}^{(1)}$ for the first order serpentine interconnect is obtained as [31]

$$\overline{T}^{(1)} = \frac{m^{(1)}}{24} \left\{ \begin{array}{ccc} 4g^3+6\pi g^2+24g+3\pi & 6(g^2+\pi g+2) & 0 \\ 6(g^2+\pi g+2) & 32[m^{(1)}]^2(2g+\pi)+8g+\pi & 48m^{(1)}(g+\pi) \\ 0 & 48m^{(1)}(g+\pi) & 24(2g+\pi) \end{array} \right\}$$

(31)

where $g = \eta^{(1)}-1$.

The second to fourth (and higher) order geometries all exhibit a rectangular geometry (shown in Fig. 1c), which indicates that, strictly speaking, the self-similarity only starts at the second order interconnects. Comparison of the self-similar serpentine structure (Fig. 1c) to the rectangular one (Fig. 1b) suggests that only their first order geometries are different. Therefore, the recursive formulae in Eqs. (29) and (30) still hold for the self-similar serpentine structure.

Substitution of $\overline{T}^{(0)}$ in Eq. (15) and $\overline{T}^{(1)}$ in Eq. (14) into Eq. (31) gives $\overline{T}^{(2)}$ as

$$\overline{T}^{(2)}(m,\eta) = \frac{m^{(2)}}{24} \left[\begin{array}{ccc} 6[\eta^{(2)}]^2(4-p)+6\left[\frac{\eta^{(2)}}{m^{(1)}}\right]^3 \overline{T}_{22}^{(1)} & 3\eta^{(2)}(p+2) & 0 \\ 3\eta^{(2)}(p+2) & 32[m^{(2)}]^2p+4p-8+6\left[\frac{\eta^{(2)}}{m^{(1)}}\right]^3 \overline{T}_{11}^{(1)} & 24m^{(2)}p \\ 0 & 24m^{(2)}p & 24p \end{array} \right]$$

(32)

where $p = \eta^{(2)}[2\eta^{(1)}+\pi-2]+2$.

Fig. 5a and b shows the components of non-dimensional flexibility vs. the order (n) for self-similar rectangular and serpentine interconnects for the height/spacing ratio $\eta = 8/\sqrt{11}$ and number of unit cell $m = 4$. The rectangular interconnect is slightly softer than the serpentine one. The analytic results are validated by FEA, which is also shown in Fig. 5a and b, for copper interconnect with the elastic modulus $E_{Cu} = 119$ GPa and Poisson's ratio $v_{Cu} = 0.34$. The component T_{13} is always zero, and is therefore not shown. The other five flexibility components all increase with n, and are more than doubled for each n increasing by 1. For n from 1 to 4, these components increase by more than 17 times, indicating that the higher order interconnect becomes much softer than the lower order one.
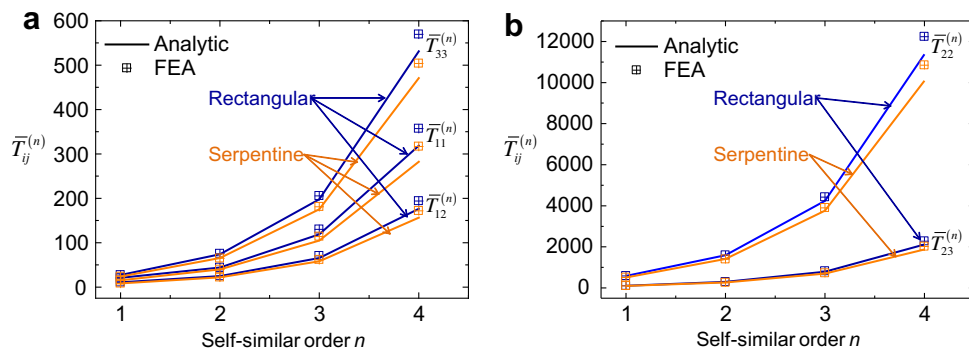

Fig. 5. The effect of self-similar order on the flexibility: the dimensionless flexibility components $\left(\overline{T}_{11}^{(n)}, \overline{T}_{12}^{(n)} \text{ and } \overline{T}_{33}^{(n)}\right)$ (a) and $\left(\overline{T}_{22}^{(n)} \text{ and } \overline{T}_{23}^{(n)}\right)$ (b) vs. the self-similar order. In the FEA, the width is fixed as $w = 0.4l^{(1)}$ for the structures of different orders.

4. Stretchability

The interconnect usually spans the space between two rigid device islands (e.g. in Fig. 1a), corresponding to clamped boundary conditions at the two ends. For stretching u_0 of the self-similar interconnect (with n orders), the boundary conditions are $u = u_0$, $v = 0$ and $\theta = 0$, and Eq. (13) then gives the reaction forces, N and Q, and bending moment M as

$$
\begin{Bmatrix} N \\ Q \\ M \end{Bmatrix} = \frac{EI}{\left[l^{(n)} \right]^3} \frac{u_0}{\overline{T}_{11}^{(n)} \overline{T}_{22}^{(n)} \overline{T}_{33}^{(n)} - \overline{T}_{11}^{(n)} \left[\overline{T}_{23}^{(n)} \right]^2 - \overline{T}_{33}^{(n)} \left[\overline{T}_{12}^{(n)} \right]^2}
$$
$$
\times \begin{Bmatrix} \overline{T}_{22}^{(n)} \overline{T}_{33}^{(n)} - \left[\overline{T}_{23}^{(n)} \right]^2 \\ -\overline{T}_{12}^{(n)} \overline{T}_{33}^{(n)} \\ l^{(n)} \overline{T}_{12}^{(n)} \overline{T}_{23}^{(n)} \end{Bmatrix}
\tag{33}
$$

since $\overline{T}_{13}^{(n)} = 0$. The maximum strains for the rectangular and serpentine configurations are analyzed separately in Sections 4.1 and 4.2. Since no experiment result is available regarding the stretchability of relative thick self-similar rectangular or serpentine interconnects, we only compare the analytic results to the finite element analysis (FEA) results for validation. The experimental measurement of the stretchability and comparison to analytic results will be considered in our future work.

4.1. Generalized self-similar rectangular interconnects

For the first order rectangular interconnect, it can be shown that the maximum strain occurs at the third nearest corners from the loading points, as illustrated in Fig. S.1a (Electronic Supplementary material), which is well supported by FEA results. The maximum strain in the interconnect can be then obtained accurately as

$$
\varepsilon_{\max} = \frac{w \left[2M + N h^{(1)} + 2Q l^{(1)} \right]}{4EI}
\tag{34a}
$$

For higher order structures with $n \geq 2$, the maximum strain can be well approximated by

$$
\varepsilon_{\max} \approx \frac{w \left[2M + N h^{(n)} + 2Q l^{(n)} - Q h^{(n-1)} \right]}{4EI} \quad (\text{for} \quad n \geq 2)
\tag{34b}
$$

Based on the yield criterion $\varepsilon_{\max} = \varepsilon_{yield}$, where ε_{yield} is the yield strain of the interconnect material (e.g. 0.3% for copper [35]), the stretchability of the generalized self-similar rectangular interconnect is obtained as

$$
\varepsilon_{stretchability}^{(1)} = \frac{\varepsilon_{yield} l^{(1)}}{w} \frac{\eta^{(1)}}{12}
$$
$$
\times \frac{16 \left[m^{(1)} \right]^2 \left[\eta^{(1)} + 1 \right] \left[\eta^{(1)} + 3 \right] - \left[\eta^{(1)} + 6 \right]^2}{4 \left[m^{(1)} \right]^2 \left[\eta^{(1)} + 1 \right] + 3 m^{(1)} \left[\eta^{(1)} + 2 \right] - \eta^{(1)} - 6}
\tag{35a}
$$

$$
\varepsilon_{stretchability}^{(n)} = \frac{\varepsilon_{yield} l^{(n)}}{w} \frac{2}{m^{(n)}} \left| \frac{\overline{T}_{11}^{(n)} \left[\overline{T}_{23}^{(n)} \right]^2 + \overline{T}_{33}^{(n)} \left[\overline{T}_{12}^{(n)} \right]^2 - \overline{T}_{11}^{(n)} \overline{T}_{22}^{(n)} \overline{T}_{33}^{(n)}}{2 \overline{T}_{12}^{(n)} \left[\overline{T}_{33}^{(n)} - \overline{T}_{23}^{(n)} \right] + \left\{ \left[\overline{T}_{23}^{(n)} \right]^2 - \overline{T}_{22}^{(n)} \overline{T}_{33}^{(n)} \right\} \eta^{(n)} - \frac{\eta^{(n-1)} \eta^{(n)}}{2 m^{(n-1)}} \overline{T}_{12}^{(n)} \overline{T}_{33}^{(n)}} \right|
$$
$$
(\text{for } n \geq 2)
\tag{35b}
$$

When the applied strain is smaller than the stretchability, the interconnect undergoes linear, reversible deformations, and no plastic deformation would accumulate, such that the interconnect would not suffer from plastic fatigue under cyclic loadings. Eqs. (35a) and (35b) show clearly that the stretchability is linearly proportional to $\varepsilon_{yield} l^{(n)}/w$. Therefore, in order to enhance the stretchability, it is better to adopt a metallic material with high yield strength and relative low elastic modulus to give a high yield strain, such as the nano-grained-size copper, or transforming metal nanocomposites [36].

4.2. Generalized self-similar serpentine interconnects

For first order serpentine interconnect, as shown in Fig. S.1b (Electronic Supplementary material), the maximum strain always occurs at the nearest or second nearest half circle from the two ends. Let $\varphi(0 \leqslant \varphi \leqslant \pi)$ represent the location of this half circle. The bending strain on the circle can be given by

$$
\varepsilon(\varphi) = \frac{w \left\{ 2M + N \left[h^{(1)} - l^{(1)} \right] + 3Q l^{(1)} + l^{(1)} (N \sin\varphi - Q \cos\varphi) \right\}}{4EI}
\tag{36}
$$

It reaches the maximum at $\varphi = \tan^{-1}(-N/Q)$, and the maximum strain is given by

$$
\varepsilon_{\max} = \frac{w \left\{ 2M + N \left[h^{(1)} - l^{(1)} \right] + 3Q l^{(1)} + l^{(1)} \sqrt{N^2 + Q^2} \right\}}{4EI}
\tag{37}
$$

The stretchability of the first order serpentine interconnect is then obtained as (via Eq. (33)):

$$
\varepsilon_{stretchability} = \frac{2 \varepsilon_{yield} l^{(1)}}{m^{(1)} w} \frac{\overline{T}_{11}^{(1)} \overline{T}_{22}^{(1)} \overline{T}_{33}^{(1)} - \overline{T}_{11}^{(1)} \left[\overline{T}_{23}^{(1)} \right]^2 - \overline{T}_{33}^{(1)} \left[\overline{T}_{12}^{(1)} \right]^2}{2 \overline{T}_{12}^{(1)} \overline{T}_{23}^{(1)} - 3 \overline{T}_{12}^{(1)} \overline{T}_{33}^{(1)} + \left\{ \overline{T}_{22}^{(1)} \overline{T}_{33}^{(1)} - \left[\overline{T}_{23}^{(1)} \right]^2 \right\} (\eta^{(1)} - 1) + \sqrt{\left\{ \overline{T}_{22}^{(1)} \overline{T}_{33}^{(1)} - \left[\overline{T}_{23}^{(1)} \right]^2 \right\}^2 + \left[\overline{T}_{12}^{(1)} \right]^2 \left[\overline{T}_{33}^{(1)} \right]^2}} .
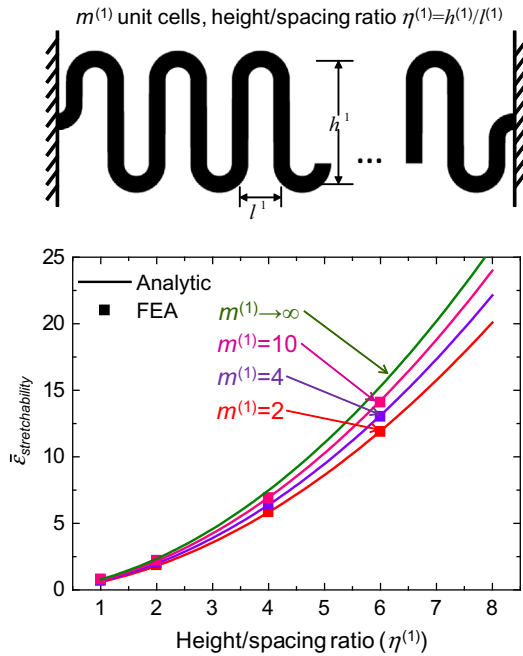\tag{38}
$$

Fig. 6. The dimensionless stretchability vs. the height/spacing ratio ($\eta^{(1)}$) for different number ($m^{(1)}$) of unit cells for the first order serpentine interconnect.

The normalized stretchability $\varepsilon_{stretchability}w/[\varepsilon_{yield}l^{(1)}]$ depends only on the height/spacing ratio $\eta^{(1)}$ and number of unit cell $m^{(1)}$. It increases with both $\eta^{(1)}$ and $m^{(1)}$, as shown in Fig. 6, and saturates to

$$\varepsilon_{stretchability} = \frac{\varepsilon_{yield}l^{(1)}}{w} \cdot \frac{4[\eta^{(1)}]^3 + 6(\pi-2)[\eta^{(1)}]^2 - 12(\pi-3)\eta^{(1)} + 9\pi - 28}{12\eta^{(1)}} \tag{39}$$

for $m^{(1)} \to \infty$ (also shown in Fig. 6).
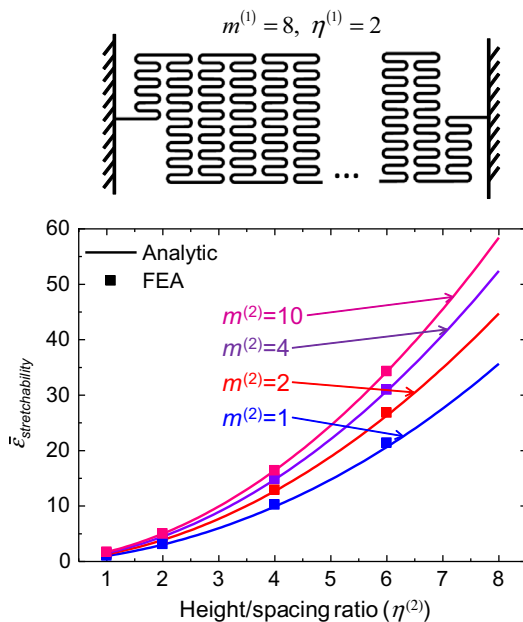
Fig. 7. The dimensionless stretchability of the second order serpentine interconnect vs. the height/spacing ratio ($\eta^{(2)}$) for different number ($m^{(2)}$) of unit cells, with ($m^{(1)}, \eta^{(1)}$) = (8, 2).
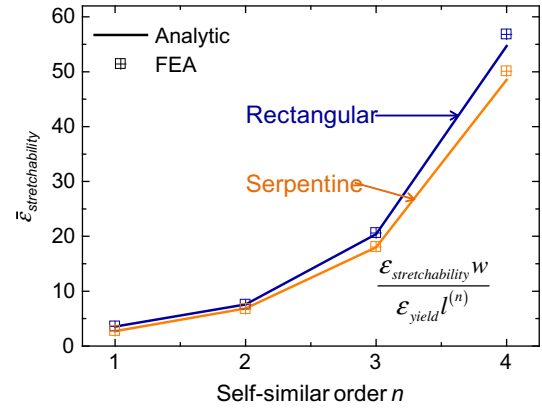

Fig. 8. The dimensionless stretchability as a function of the self-similar order. In the FEA, the width is fixed as $w = 0.4l^{(1)}$ for the structures of different orders.

For higher order ($n \geqslant 2$) serpentine interconnects, Eq. (35b), together with the corresponding flexibility matrix $\overline{T}^{(2)}$ in Eq. (32) and $\overline{T}^{(n)}$ in Eq. (30) for serpentine interconnects, give an excellent approximation to the stretchability as compared to the FEA shown in Fig. 7.

Fig. 8 shows the normalized stretchability, $\varepsilon_{stretchability}w/[\varepsilon_{yield}l^{(n)}]$, vs. the order n for self-similar rectangular and serpentine interconnects, where the height/spacing ratio $\eta = 8/\sqrt{11}$ and number of unit cell $m = 4$ at different orders. The stretchability is more than doubled for each n increasing by 1, indicating the elastic limit of the interconnect can be well improved by adopting higher order self-similar design. Fig. 8 also shows that the analytic model agrees very well with the FEA results.

The analytic models and FEA results above are all for infinitesimal deformation. Table S.1 (Electronic Supplementary material) shows that the effect of finite deformation on stretchability (determined by FEA) is negligible for both first and second order serpentine interconnects, with various combinations of geometric parameters. Therefore, the analytic models above give good estimations of the stretchability. In real fabrications, the microscale self-similar serpentine interconnect may have imperfections due to lithography defects, especially along the sidewalls of the lines, and such geometric imperfections will increase for decreased pattern size (i.e. metal width and rounding radius) that may occur when increasing the self similar order. These geometric imperfections are not accounted for in the present study.

5. Optimal design of self-similar serpentine interconnects for stretchable electronics

Two competing goals of stretchable electronics [19,37] are (1) high surface filling ratio of active devices, which requires small spacing between the device islands (Fig. 9a); and (2) large stretchability of the system, which demands large spacing between the device islands. Prior approaches based on buckling of straight or conventional serpentine interconnects achieve ~100% stretchability
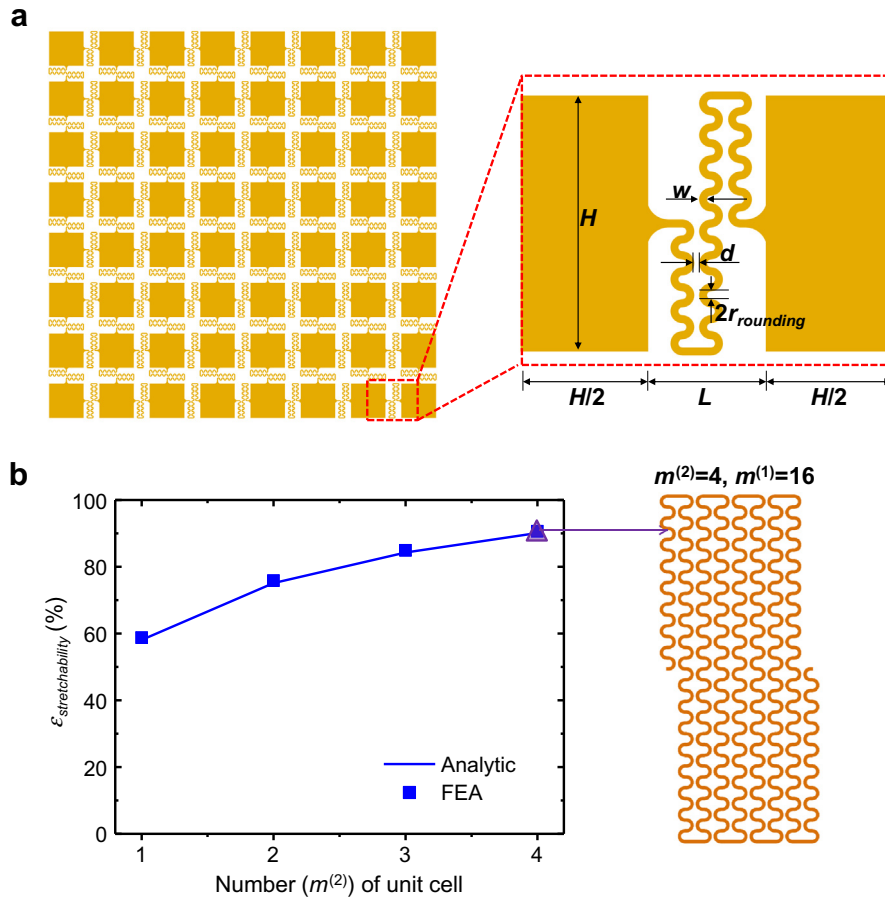
Fig. 9. Design optimization of the second order serpentine interconnects for island–bridge structure. (a) Schematic of the island–bridge structure with a 8 × 8 array, and illustration on the geometric parameters; (b) the maximum stretchability vs. the number ($m^{(2)}$) of unit cells (left panel), and the optimized configuration (right panel).

[17,18,28,30]. The stretchability ($\varepsilon_{stretchability}^{system}$) of the system is related to that ($\varepsilon_{stretchability}^{interconnect}$) of the interconnect by

$$\varepsilon_{stretchability}^{system} = \varepsilon_{stretchability}^{interconnnect}\left(1 - \sqrt{f}\right) \qquad (40)$$

where f denotes the surface filling ratio. For $\sim$50% surface filling ratio of active devices, the $\sim$100% stretchability of the interconnect translates to $\sim$30% stretchability of the system, which is low for some biomedical applications of stretchable electronics (to skin, heart or elbow). The analytic models in Sections 3 and 4 can guide the design of generalized self-similar interconnects to simultaneously achieve the two competing goals above.

The second order serpentine interconnects are studied to illustrate the design optimization in a square-shaped device island with a representative size $H = 1$ mm and the surface filling ratio of 50% (Fig. 9a). The photolithography technology [38,39] for fabricating the metal interconnect poses some constraints, such as the width $w \geqslant 10$ μm, rounding radius $r_{rounding} \geqslant 10$ μm and the distance between neighboring arcs $d \geqslant 5$ μm (Fig. 9a). Other geometric parameters are optimized to achieve large stretchability. Fig. 9b shows that the stretchability increases with the number of unit cells $m^{(2)}$. The right panel of Fig. 9b shows the optimal

design, which gives $\sim$308% stretchability of the interconnect, and corresponds to $\sim$90% stretchability of the system, outperforming the previous designs using buckled interconnects [18,28]. Even for a much larger surface filling ratio 70%, Eq. (40) still gives $\sim$50% stretchability of the system.

6. Conclusions

This paper develops the analytic models of flexibility and stretchability for the self-similar interconnects. After the straightforward design optimization, the analytic models, validated by FEA, show that the higher order self-similar interconnect gives very large stretchability of the system, such as $\sim$90% for 50% surface filling ratio of active devices, or >50% stretchability for 70% surface filling ratio. The analytic models are useful for the development of stretchable electronics that simultaneously demand large areal coverage of active devices, such as stretchable photovoltaics [11] and electronic eyeball cameras [12]. The concept of self-similar serpentine configuration could be further combined with other strategies of stretchability enhancement, e.g. the control of wrinkling patterns, to give an enhanced level of stretchability for interconnects bonded to the substrate.

Appendix A. Supplementary material

Supplementary data associated with this article can be found, in the online version, at http://dx.doi.org/10.1016/j.actamat.2013.09.020.

References

[1] Lacour SP, Jones J, Wagner S, Li T, Suo ZG. Proc IEEE 2005;93:1459.
[2] Lacour SP, Wagner S, Huang ZY, Suo Z. Appl Phys Lett 2003;82:2404.
[3] Lacour SP, Wagner S, Narayan RJ, Li T, Suo ZG. J Appl Phys 2006;100:014913.
[4] Khang DY, Jiang HQ, Huang Y, Rogers JA. Science 2006;311:208.
[5] Kim DH, Ahn JH, Choi WM, Kim HS, Kim TH, Song JZ, et al. Science 2008;320:507.
[6] Sekitani T, Noguchi Y, Hata K, Fukushima T, Aida T, Someya T. Science 2008;321:1468.
[7] Sekitani T, Nakajima H, Maeda H, Fukushima T, Aida T, Hata K, et al. Nat Mater 2009;8:494.
[8] Kim DH, Lu NS, Ma R, Kim YS, Kim RH, Wang SD, et al. Science 2011;333:838.
[9] Song YM, Xie YZ, Malyarchuk V, Xiao JL, Jung I, Choi KJ, et al. Nature 2013;497:95.
[10] Duan YQ, Huang YA, Yin ZP. Thin Solid Films 2013;544:152.
[11] Yoon J, Baca AJ, Park SI, Elvikis P, Geddes JB, Li LF, et al. Nat Mater 2008;7:907.
[12] Ko HC, Stoykovich MP, Song JZ, Malyarchuk V, Choi WM, Yu CJ, et al. Nature 2008;454:748.
[13] Wagner S, Lacour SP, Jones J, Hsu PHI, Sturm JC, Li T, et al. Physica E 2004;25:326.
[14] Someya T, Sekitani T, Iba S, Kato Y, Kawaguchi H, Sakurai T. Proc Natl Acad Sci USA 2004;101:9966.
[15] Mannsfeld SCB, Tee BCK, Stoltenberg RM, Chen C, Barman S, Muir BVO, et al. Nat Mater 2010;9:859.
[16] Saeidpourazar R, Li R, Li YH, Sangid MD, Lu CF, Huang YG, et al. J Microelectromech Syst 2012;21:1049.
[17] Kim DH, Song JZ, Choi WM, Kim HS, Kim RH, Liu ZJ, et al. Proc Natl Acad Sci USA 2008;105:18675.
[18] Lee J, Wu JA, Shi MX, Yoon J, Park SI, Li M, et al. Adv Mater 2011;23:986.
[19] Xu S, Zhang YH, Cho J, Lee J, Huang X, Jia L, et al. Nat Commun 2013;4:1543.
[20] Kim RH, Tao H, Kim TI, Zhang YH, Kim S, Panilaitis B, et al. Small 2012;8:2812.
[21] Jones J, Lacour SP, Wagner S, Suo ZG. J Vac Sci Technol A 2004;22:1723.
[22] Gonzalez M, Axisa F, Bossuyt F, Hsu YY, Vandevelde B, Vanfleteren J. Circuit World 2009;35:22.
[23] Gonzalez M, Axisa F, BuIcke MV, Brosteaux D, Vandevelde B, Vanfleteren J. Microelectron Reliab 2008;48:825.
[24] van der Sluis O, Hsu YY, Timmermans PHM, Gonzalez M, Hoefnagels JPM. J Phys D – Appl Phys 2011;44:034008.
[25] Hsu YY, Gonzalez M, Bossuyt F, Axisa F, Vanfleteren J, De Wolf I. J Mater Res 2009;24:3573.
[26] Hsu YY, Gonzalez M, Bossuyt F, Axisa F, Vanfleteren J, DeWolf I. J Micromech Microeng 2010;20:075036.
[27] Hsu YY, Gonzalez M, Bossuyt F, Vanfleteren J, De Wolf I. IEEE Trans Electron Dev 2011;58:2680.
[28] Lee J, Wu J, Ryu JH, Liu ZJ, Meitl M, Zhang YW, et al. Small 2012;8:1851.
[29] Sun YG, Choi WM, Jiang HQ, Huang YGY, Rogers JA. Nat Nanotechnol 2006;1:201.
[30] Kim DH, Liu ZJ, Kim YS, Wu J, Song JZ, Kim HS, et al. Small 2009;5:2841.
[31] Zhang YH, Xu S, Fu HR, Lee J, Su J, Hwang KC, et al. Soft Matter 2013;9:8062.
[32] Kim DH, Wang SD, Keum H, Ghaffari R, Kim YS, Tao H, et al. Small 2012;8:3263.
[33] Su YW, Wu J, Fan ZC, Hwang KC, Song JZ, Huang YG, et al. J Mech Phys Solids 2012;60:487.
[34] Timoshenko S, Gere J. Theory of elastic stability. New York: McGraw-Hill; 1961.
[35] William FR, Leroy DS, Don HM. Mechanics of materials. New York: Wiley; 1999.
[36] Hao SJ, Cui LS, Jiang DQ, Han XD, Ren Y, Jiang J, et al. Science 2013;339:1191.
[37] Rogers JA, Someya T, Huang YG. Science 2010;327:1603.
[38] Meitl MA, Zhu ZT, Kumar V, Lee KJ, Feng X, Huang YY, et al. Nat Mater 2006;5:33.
[39] Carlson A, Bowen AM, Huang YG, Nuzzo RG, Rogers JA. Adv Mater 2012;24:5284.